Journal of Power Sources 196 (2011) 8004–8011

Contents lists available at ScienceDirect

Journal of Power Sources

journal homepage: www.elsevier.com/locate/jpowsour

Numerical study on the evaporative and condensational dissipation of phosphoric acid in PAFC

Haruhiko Hirata[a,*], Tsutomu Aoki[b], Kazuyoshi Nakajima[c]

[a] Plant Engineering Dept., Thermal & Hydro Power Systems & Services Div., Toshiba Corporation, 2-4, Suehiro-cho, Tsurumi-ku, Yokohama 230-0045, Japan
[b] Development Dept., Toshiba Fuel Cell Power System Corporation, Japan
[c] Metals Technology R&D Dept., Power & Industrial Systems R&D Center, Toshiba Corporation, Japan

ARTICLE INFO

Article history:
Received 18 February 2011
Received in revised form 15 April 2011
Accepted 11 May 2011
Available online 19 May 2011

Keywords:
Phosphoric acid fuel cell
Evaporation
Condensation
Two components nucleation theory
Numerical analysis

ABSTRACT

In phosphoric acid fuel cell (PAFC) stack, reduction of the phosphoric acid that is impregnated in the cell is a major factor to restrict the operating life. In this paper, the phosphoric acid reduction by the evaporative and condensational dissipation was evaluated by numerical analysis. The calculations that include the behavior of heat transfer, gas flow, and evaporation and condensation of phosphoric acid were conducted for the model cell with conditions that correspond to an on site stack. The phosphoric acid was considered as a composite of phosphorus pentoxide and water, and the evaporation and condensation rates were derived based on the nucleation theory for a two components system. The phosphoric acid distributions in the vapor phase and liquid phase at the process gas and electrode were calculated for the duration of 3300 h, and as a result of those, the exhausting and remaining amount of phosphoric acid for the cell were evaluated. The analysis results were compared with the experimental results for the model cell.

1. Introduction

In phosphoric acid fuel cell (PAFC) stack, phosphoric acid that has low vapor pressure is used as an electrolyte to suppress the evaporation and dissipation with the process gases (the fuel and oxidant gases). However, the decrease in cell performance as a result of the reduction of phosphoric acid is not negligible at the operating temperature of about 200 °C. For stacks that are designed to have an operating life of over 40,000 h, a basic design to keep low temperature at the gas exit comparing with the gas inlet of the cell is adopted. As a result of the design, the evaporated phosphoric acid in the process gas is condensed and recovered to the cell at the gas exit.

Yoshioka et al. have conducted experimental and numerical studies for evaporation [1] and condensation [2] of phosphoric acid. In those studies, the evaporation rate was treated to be controlled by the diffusion rate in the concentration boundary layer of process gas and the condensation rate was treated to be controlled by the cooling rate of process gas, and the phosphoric acid distributions in vapor and liquid phases and the recovery of phosphoric acid for the model cell were discussed.

In general, the vapor pressure of phosphoric acid in the process gas is different from the saturated vapor pressure, as the evaporation and condensation rates between the cell and process gas have limited values. Furthermore, the partial pressure of phosphoric acid in the process gas is determined by complex balance of evaporation and condensation rates and passing duration time of process gas that go through the cell channel. Therefore, a detailed design method that includes such complex mechanisms was required to estimate the amount of the dissipation of phosphoric acid precisely. Besides, to predict the phosphoric acid distribution in the cell with the time progress is important to estimate the degradation of cell performance.

In the present paper, numerical analysis that include the behavior of the heat transfer, gas flow, and evaporation and condensation of phosphoric acid were conducted for the model cell that consists of porous electrode substrate and matrix. The evaporation and condensation rate of phosphoric acid were calculated based on the nucleation theory for a two components system. The conditions of the temperature and impregnated phosphoric acid concentration for the model cell were correspondent with those of an on site cell, and time series solutions for the duration of 3300 h were calculated. The phosphoric acid distributions in the vapor phase and liquid phase at the process gas and cell were calculated, and as a result of those, the exhausting and remaining phosphoric acid for the cell were calculated, and the results were evaluated by comparing with the results for the model cell experiment.

2. Analysis method

The analysis code that was developed for a PAFC stack was used for the calculations. The code is based on the analysis code that

* Corresponding author. Tel.: +81 45 500 1539; fax: +81 45 500 1594.
E-mail address: haruhiko.hirata@toshiba.co.jp (H. Hirata).

0378-7753/$ – see front matter © 2011 Elsevier B.V. All rights reserved.
doi:10.1016/j.jpowsour.2011.05.018

Nomenclature

List of symbols

J	evaporated or condensed phosphoric acid flux ($mol\,s^{-1}\,cm^{-2}$)
$\Delta\tilde{G}^*$	activation energy change ($J\,mol^{-1}\,K^{-1}$)
$\tilde{c}$	frequency factor
c_E	frequency factor coefficient for evaporation
c_C	frequency factor coefficient for condensation
P_a	partial pressure of phosphorus pentoxide
P_{sa}	saturated vapor pressure of phosphorus pentoxide
R	universal gas constant ($8.314\,J\,mol^{-1}\,K^{-1}$)
k	Boltzmann constant (1.38E−23 J)
t	temperature (°C)
T	absolute temperature (K)
x	molar fraction
μ	chemical potential ($J\,mol^{-1}$)
γ	activity coefficient
β	collision rate

Subscripts

a	phosphorus pentoxide
w	water
g	vapor phase
l	liquid phase
E	evaporation
C	condensation
s	saturation

Superscript

0	pure component

has been developed for the characteristic calculation of a molten carbonate fuel cell (MCFC) stack [3], and the function of electrode reaction has modified to correspond to that of the PAFC and the functions for the evaporation and condensation of phosphoric acid have been added. Therefore, the analysis features about the heat transfer and gas flow are the same as those of the code for MCFC.

The phosphoric acid migrations in PAFC stack are considered to be caused by the following two mechanisms.

(1) Migration accompanied with the phase change between liquid and vapor. That is dissipation of phosphoric acid from the porous electrode to process gas by evaporation and recovery from the process gas to porous electrode by condensation with the transfer by gas flow.
(2) Migration in the liquid phase. That is migration by capillary force caused by the concentration or temperature change of phosphoric acid in the porous electrode.

In this paper, the phenomenon above (1) that has main effect for exhausting of phosphoric acid was considered in the calculation. The phosphoric acid was regarded as a two components system of phosphorus pentoxide (P_4O_{10}) and water (H_2O), and the evaporation and condensation rates of phosphoric acid between the cell and process gas were considered to have limited values, and these were expressed by the following activation process based on the nucleation (droplet condensation) theory of a two components system in Refs. [8–10]:

$$J = \tilde{c}\,\exp\left(\frac{-\Delta\tilde{G}^*}{RT}\right) \tag{1}$$

Here, J is the amount of evaporating or condensing phosphoric acid $mol\,s^{-1}\,cm^{-2}$ per unit area and unit time on the electrode surface, R is the universal gas constant $8.314\,J\,mol^{-1}\,K^{-1}$, T is the liquid phase absolute temperature K, $\Delta\tilde{G}^*$ is the activation energy $J\,mol^{-1}$, and $\tilde{c}$ is the frequency factor.

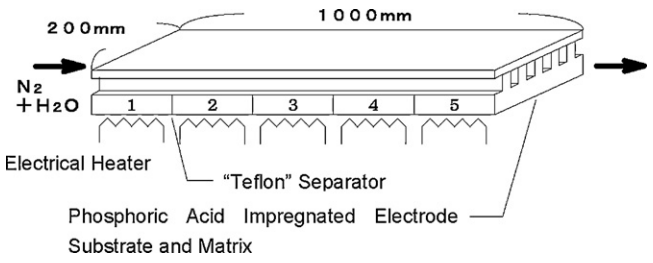

Fig. 1. Outline of model cell experiment.

The calculation methods of evaporation and condensation rates will be mentioned in Appendix A. Whereas saturated vapor pressure of P_4O_{10} and H_2O were derived by the vapor liquid equilibrium for a two components system, and the activation energy were derived from the temperature and composition for the vapor phase and liquid phase of phosphoric acid in the process gas and cell based on the free energy change with phase change. The concentrations of P_4O_{10} and H_2O in the evaporating or condensing phosphoric acid were also determined from the free energy changes. The dependencies of the temperature and concentration of P_4O_{10} and H_2O on the frequency factor were derived from the Hertz–Knudsen equation, and the frequency factor coefficients were determined so as to meet the analysis results with the experimental results, as it will be mentioned later.

Whether evaporation or condensation arises on the electrode surface was determined by comparing P_4O_{10} partial pressure P_a in vapor phase at the process gas with P_4O_{10} saturated vapor pressure P_{sa} that was determined by the composition and temperature in liquid phase at the electrode as follows:

$$P_a < P_{sa};\ \text{Evaporation} \tag{2}$$

$$P_a > P_{sa};\ \text{Condensation} \tag{3}$$

The code for MCFC is an analysis program that performs repetition calculation and acquires a steady state solution about the phenomena that are the results of coupling for the electrochemical reaction, heat transfer, and gas flow. However, the code for PAFC was required to calculate the time variation of phosphoric acid dissipation under the various temperature, vapor phase composition, and liquid phase composition. Therefore, the unsteady analysis loop that includes the analysis loop of the code for MCFC was programmed, and the evaporation and condensation rates and the amount of phosphoric acid in the vapor phase and liquid phase at the process gas and electrode were calculated in this unsteady loop. The calculation for the balance of phosphoric acid in unsteady analysis loop will be mentioned in Appendix B.

3. Analysis conditions

Analysis was conducted on the conditions that correspond to the following model cell experiment. The outline of the experiment is shown in Fig. 1, and the experimental conditions are shown in Table 1. The experiment was carried out using the porous electrode substrate and matrix in that phosphoric acid was impregnated, and the steam humidified N_2 gas that was substitute process gas was run through the electrode gas channel. The temperature in each electrode section was controlled by an electrical heater to represent the cell temperature distribution along the oxidant gas flow for an on site stack. The phosphoric acid migration as liquid phase between the electrode sections was prevented by "Teflon" boards between each section. The amount of the remain-

Table 1
Experiment and analysis conditions.

Pressure		1 atm				
Gas flow rate		N_2 (3.5 l min^{-1}) + 60 °C humidified				
Operation duration		3300 h				
Initial phosphoric acid amount		11.4 cm^3 (85 wt% H_3PO_4, 25 °C)/section				
Temperature	Inlet	Section				Outlet
		1	2	3	4	5
		205 °C	205 °C	198 °C	178 °C	163 °C

ing phosphoric acid in each electrode section was derived from the quantitative analysis results by ICP-OES (Inductively Coupled Plasma Optical Emission Spectrometer) after 3300 h elapsed state. Each section was divided into nine elements, and analysis was conducted adopting one dimensional model in the direction of the gas flow. The frequency factor coefficients for evaporation and a condensation rate were determined so as to meet the remaining phosphoric acid of analysis results with that of the experimental results. At this time, the evaporation rate frequency factor coefficient c_E in Eq. (A.2.13) was determined according to the amount of remaining phosphoric acid in the 1st section of electrode, and the condensation rate frequency factor coefficient c_C in Eq. (A.2.17) was determined according to the amount of remaining phosphoric acid in the 5th section of electrode. The same frequency factor coefficient values were adopted for the 2nd, 3rd, and 4th electrode sections and the frequency factor coefficients used for the analysis were as follows:

$$c_E = -3.1E38 \quad [\mathrm{m\ s^{-1}\,kg^{1/2}\,J^{1/2}mol^{-1/2}}] \tag{4}$$

$$c_C = 3.1E-81 \quad [\mathrm{m\ s^{-1}\,kg^{1/2}\,J^{1/2}\,mol^{-1/2}Pa^{-1}}] \tag{5}$$

4. Analysis results

4.1. Evaporation and condensation rates of phosphoric acid

The evaporation and condensation rate distributions of phosphoric acid along the gas flow direction for the initial state, 2000 h elapsed state, and 3300 h elapsed state are shown in Fig. 2. Here, the negative rate shows evaporation and positive rate shows condensation. The evaporation arises at sections 1 and 2 (0.0–0.4 m, is the distance from the gas inlet). The condensation arises at section 5 (0.8–1.0 m, is the distance from the gas inlet) where the electrode temperature fell steeply comparing with the upstream. The peak magnitude of evaporation and condensation rate fell according to the progress of time, and the peak position of evaporation and condensation rate gradually moved to the downstream of gas flow.

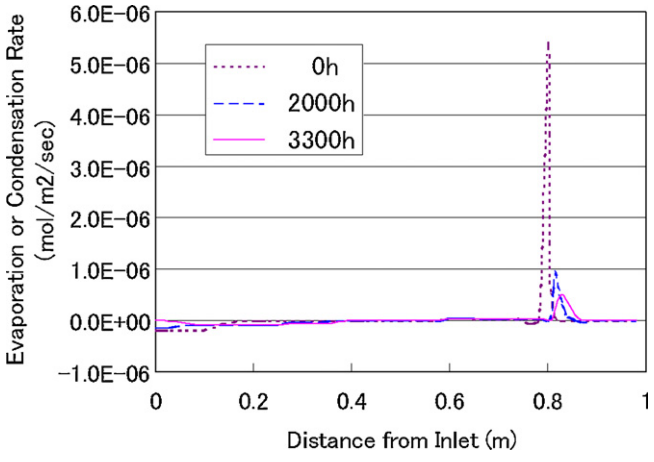

Fig. 2. Evaporation and condensation rates along the substrate (minus: evaporation, plus: condensation).

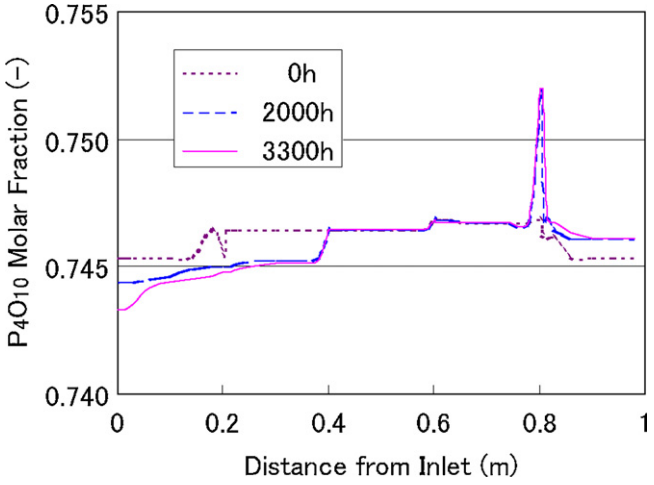

Fig. 3. P_4O_{10} molar fractions of evaporating and condensing phosphoric acid along the substrate.

The evaporation rate had gradual distributions in wide area, whereas the condensation rate had steep distributions in narrow area. These were caused by the following mechanism. The activation energy for evaporation rate was determined by thick P_4O_{10} concentration in the liquid phase at electrode and response to the gas flow change came out slowly, though activation energy for condensation rate was determined by thin P_4O_{10} partial pressure in the vapor phase at process gas and response to the gas flow change came out rapidly, as shown in Eqs. (A.2.11) and (A.2.16) respectively. These relations were also shown in the P_4O_{10} partial pressure distribution that gradually increased at the inlet and steeply decreased at the outlet for each time in Fig. 6.

P_4O_{10} molar fraction distribution of evaporating and condensing phosphoric acid composition along the gas flow direction is shown in Fig. 3. P_4O_{10} molar fraction of evaporating composition at sections 1 and 2 fell according to the time progress, but there was few change in P_4O_{10} molar fraction from 0.746 at initial state to 0.744 at 3300 h elapsed state. In condensing composition at section 5, P_4O_{10} molar fraction increased according to the time progress, but the change was also a few and it was from 0.746 at initial state to 0.752 at 3300 h elapsed state. P_4O_{10} concentration of evaporating and condensing compositions that were determined by Eq. (A.2.10) were thicker comparing with the phosphoric acid molar fraction 0.0922 (85 wt% H_3PO_4) that was impregnated in the electrode at the initial state.

4.2. Amount of phosphoric acid in liquid phase at the electrode

P_4O_{10} and H_2O molar concentration distributions in liquid phase at electrode along the gas flow direction are shown in Fig. 4. The molar concentration of P_4O_{10} and H_2O decreased gradually at sections 1 and 2 by evaporation, and increases steeply at section 5 by condensation with the progress of time. Since P_4O_{10} concentrations of evaporating and condensing phosphoric acid were thicker than that of impregnated phosphoric acid in the electrode, the variation of P_4O_{10} concentration in liquid phase at electrode was larger than the variation of H_2O concentration at sections 1, 2, and 5. The peak position of evaporation and condensation rate moved toward the gas downstream, and the evaporation and condensation rate decreased with the time progress in Fig. 2. These were correspondent with the decrease and increase of the molar concentration of

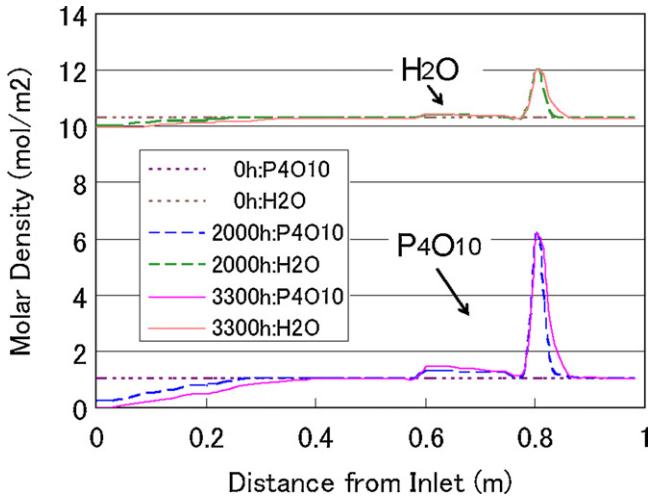

Fig. 4. P_4O_{10} and H_2O molar density of liquid phase in the electrode.

P_4O_{10} and H_2O in the liquid phase according to the gas flow for the evaporation and condensation respectively in Fig. 4.

The amount of remaining P_4O_{10} in each electrode section at 3300 h elapsed state for the analysis results and experimental results are shown in Fig. 5. As mentioned in the chapter 3, the frequency factor coefficient of evaporation rate was determined so as to meet the remaining P_4O_{10} of analysis result in section 1 with that of experimental results, and the frequency factor coefficient of condensation rate was determined so as to meet the remaining P_4O_{10} of analysis result in section 5 with that of experimental results. Regarding the frequency factor coefficients for sections 2–4, the same frequency factor coefficients of sections 1 and 5 were adopted, and as a result of those, the amount of remaining P_4O_{10} for sections 2–4 were calculated with good meet to the experimental results. Therefore, adopting appropriate frequency factor coefficients for the evaporation and condensation rates, the phosphoric acid dissipation for other temperature and gas flow conditions was estimated to be calculated accurately by the analysis method that mentioned in the present paper.

The amount of remaining P_4O_{10} for the analysis and experimental results increased according to the section goes to the gas outlet direction. Especially in sections 4 and 5, there were much P_4O_{10} comparing with the impregnated P_4O_{10}, and the recovery of phosphoric acid from the process gas by condensation was observed.

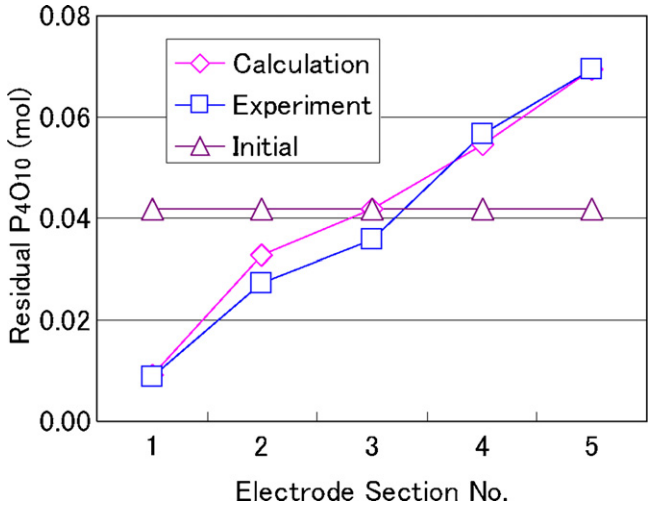

Fig. 5. Residual P_4O_{10} in the electrode after 3300 h.

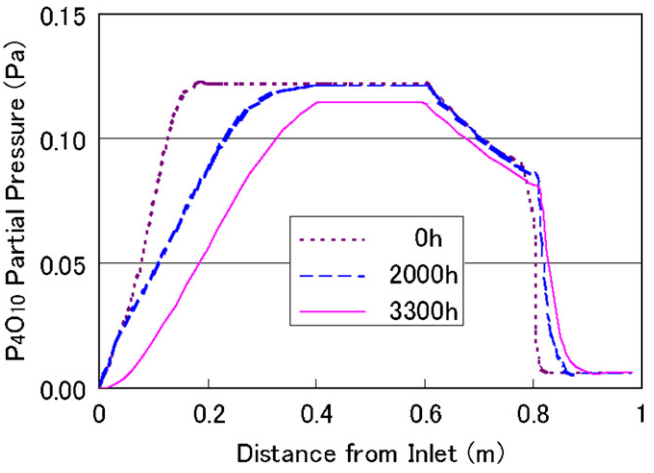

Fig. 6. P_4O_{10} partial pressure along the substrate.

4.3. Partial pressure and saturated vapor pressure of phosphoric acid

P_4O_{10} partial pressure and H_2O partial pressure distributions of vapor phase in the process gas along the gas flow direction at initial state, 2000 h and 3300 h elapsed states are shown in Figs. 6 and 7 respectively.

At the initial state, the partial pressure of P_4O_{10} and H_2O increased along the gas flow and reached to saturation in section 1 where evaporation occurred, and decreased along the gas flow and reached to fixed values in sections 4 and 5 where condensation occurred. The gradual increases at section 1 and the steep decrease at section 5 for P_4O_{10} and H_2O partial pressures were correspondent to the gradual decrease of the evaporation rate at section 1 and the steep increase of condensation rate at section 5 in Fig. 2. The increase of P_4O_{10} and H_2O partial pressures at the gas inlet part became loose according to the progress of time, and the distance between the gas inlet and the position where the vapor pressure reached to saturation became long. P_4O_{10} partial pressure at the gas exit that determines the amount of exhausting phosphoric acid was almost stable around 6.03E−3 Pa in the progress of time. H_2O partial pressure slightly increased from 6.88E−4 Pa at initial state to 7.73E−4 Pa at 3300 h elapsed state.

P_4O_{10} partial pressure in the vapor phase and P_4O_{10} saturated vapor pressure that was determined by the condition in liquid phase at electrode at initial state and 3300 h elapsed state are shown in Figs. 8 and 9 respectively.

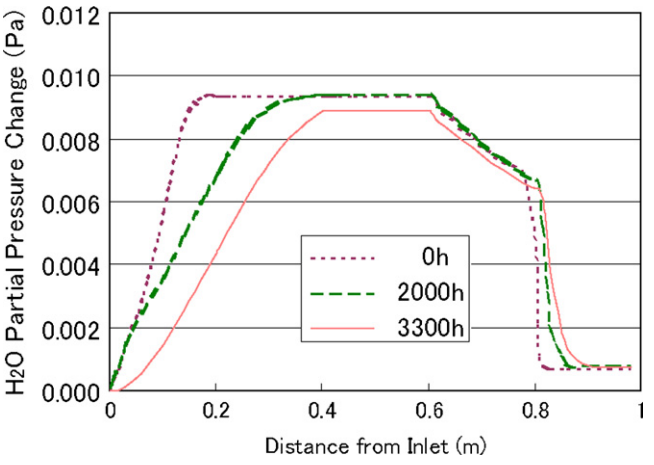

Fig. 7. H_2O partial pressure change along the substrate.

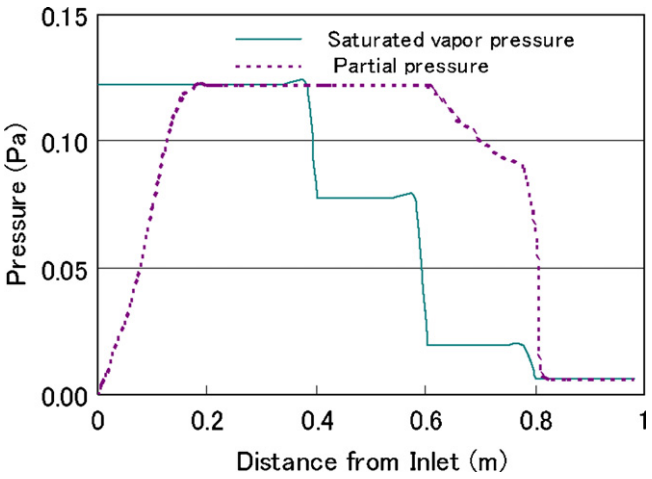

Fig. 8. P_4O_{10} saturated vapor pressure and partial pressure along the substrate at initial state.

At the initial state, P_4O_{10} partial pressure at the gas inlet part was lower than the saturated vapor pressure and according to the gas flow, after that the partial pressure increased and reached to saturation. At sections 3 and 4 where the distance from the gas inlet part are from 0.4 to 0.8 m, P_4O_{10} partial pressure was higher than the saturated vapor pressure and the vapor phase of process gas was supersaturating state regarding to the temperature and phosphoric acid concentration in the liquid phase at the electrode. At section 5 where the distance from the gas inlet is 0.8 m or more, P_4O_{10} partial pressure decreased steeply and reached to saturated vapor pressure according to the liquid phase conditions at the gas exit.

At the 3300 h elapsed state, P_4O_{10} saturated vapor pressure increased from 0 according to the gas flow, and P_4O_{10} partial pressure distribution was almost equal to the saturated vapor pressure distribution in sections 1 and 2. P_4O_{10} saturated vapor pressure decreased comparing to the initial state, as the liquid phase phosphoric acid concentration was decreased because of the thicker evaporating P_4O_{10} concentration as shown in Fig. 3. P_4O_{10} partial pressure was supersaturating state at sections 3 and 4, and it decreased steeply at section 5 and reached to the saturated vapor pressure at the gas exit. The saturated vapor pressure steeply rose at the gas inlet portion of section 5 caused by the steep increase of P_4O_{10} concentration in the electrode by condensation as shown in Fig. 4.

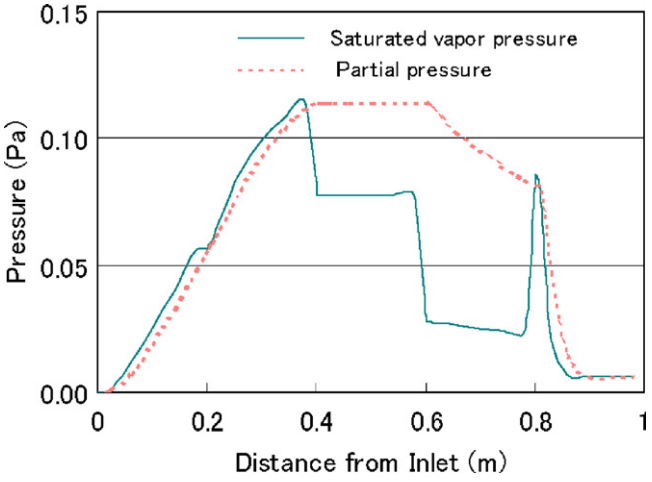

Fig. 9. P_4O_{10} saturated vapor pressure and partial pressure along the substrate after 3300 h.

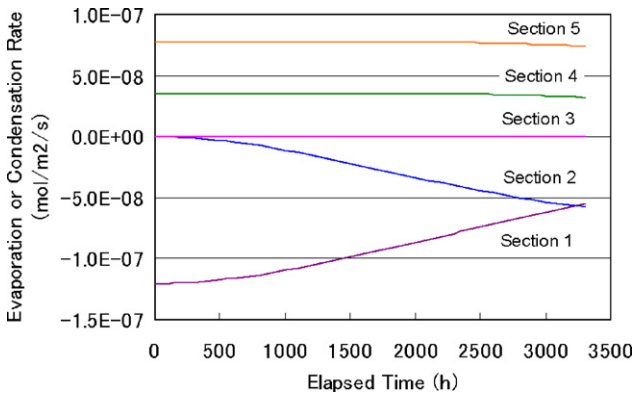

Fig. 10. Time variation of evaporation and condensation rates (minus: evaporation, plus: condensation).

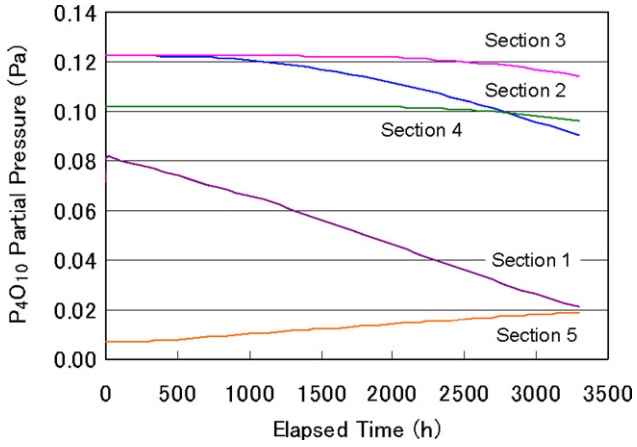

Fig. 11. Time variation of P_4O_{10} partial pressure.

4.4. Variation in the time progress

The phosphoric acid evaporation and condensation rates at each section, P_4O_{10} partial pressures in the vapor phase at process gas, the amounts of remaining P_4O_{10} in the liquid phase at electrode at each section for the variation with time progress are shown in Figs. 10–12 respectively.

Regarding the phosphoric acid evaporation and condensation rates, the average evaporation rate at section 1 decreased and

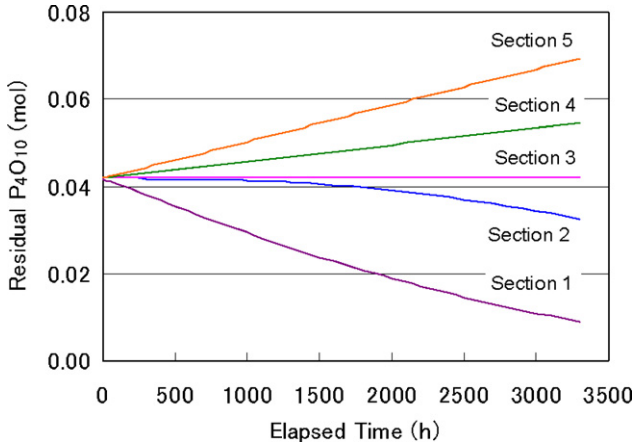

Fig. 12. Time variation of residual P_4O_{10} in the electrode.

the average evaporation rate at section 2 increased with the progress of time. These were caused by the difference between the saturated vapor pressure and the partial pressure of P_4O_{10} were decreased at section 1 and increased at section 2 with the progress of time as shown in Figs. 8 and 9 respectively. The evaporation and condensation rate at section 3 was maintained almost the same as initial state, and the average condensation rate at sections 4 and 5 decreased slightly with the progress of time.

P_4O_{10} partial pressure at sections 1 and 2 decreased with the progress of time according to the decrease of P_4O_{10} amount in the liquid phase at electrode as shown in Fig. 12. P_4O_{10} partial pressure at sections 3 and 4 was maintained almost the same until 2000 h and after that decreased slightly, these were caused by P_4O_{10} saturated vapor pressure decrease at 3300 h elapsed state comparing with the initial state as shown in Figs. 8 and 9. In section 5, P_4O_{10} partial pressure increased with the time progress caused by the increase of P_4O_{10} amount in the liquid phase at electrode as shown in Fig. 4.

The amount of P_4O_{10} reduced 0.0322 mol and 0.00930 mol in sections 1 and 2 respectively at the 3300 h elapsed state comparing with the initial state. P_4O_{10} at section 3 was maintained around 0.0419 mol through the duration of 3300 h. The amount of P_4O_{10} increased 0.0125 mol at section 4 and 0.0274 mol at section 5 at the 3300 h elapsed state comparing with the initial state. Consequently, the P_4O_{10} at sections 1 and 2 migrated to sections 4 and 5 by the evaporation and condensation accompanied with gas flow. The total remaining P_4O_{10} in the electrode reduced 0.00210 mol after 3300 h, this shows the amount of exhausted P_4O_{10} with the process gas and it was 1.0% of the total impregnated P_4O_{10} at the initial state.

5. Conclusion

The evaporative dissipation and migration characteristics of phosphoric acid in the model cell were calculated by the analysis code for PAFC that include the behavior of the heat transfer, process gas flow, and evaporation and condensation of phosphoric acid. The analysis was conducted for the model cell that consists of porous electrode substrate and matrix and has correspondent conditions with that for an on site stack in the duration of 3300 h.

The evaporation and condensation behavior of phosphoric acid were calculated based on the nucleation theory of a two components system, and consequently the phosphoric acid dissipation characteristic for each electrode section was calculated. The analysis results had good meet with the experimental results by adopting appropriate frequency factor coefficients for the evaporation and condensation rates. Consequently the effectiveness of the present analysis method was validated.

P_4O_{10} partial pressure was affected by the conditions of the vapor phase in process gas and the liquid phase in electrode, and for some conditions, P_4O_{10} partial pressure could be higher than the saturated vapor pressure according to the liquid phase in the electrode, and the supersaturating states were resulted to be possible.

The amount of remaining P_4O_{10} decreased in the high temperature sections at gas inlet side and increased in the low temperature sections at gas outlet side through the 3300 h duration. Consequently, P_4O_{10} in the gas inlet sections migrated to the gas outlet sections by the evaporation and condensation accompanied with the gas flow. Besides, 1.0% of total impregnated P_4O_{10} was exhausted with process gas after 3300 h. The remaining distribution and exhausting amount of P_4O_{10} for the electrode were estimated into the details.

Appendix A. A. Evaporation and condensation rates of phosphoric acid

A.1. The vapor liquid equilibrium of a two components system

The phosphoric acid was regarded as a two components system of phosphorus pentoxide (P_4O_{10}) and water (H_2O), and the vapor liquid equilibrium was considered. The saturated vapor pressure P_{sa} for P_4O_{10} in arbitrary concentration of phosphoric acid in the liquid phase was derived as follows:

$$P_{sa} = P^0_{sa} \cdot \gamma_a \cdot x_a \tag{A.1.1}$$

Here, P^0_{sa} is the pure P_4O_{10} saturated vapor pressure mmHg, γ_a and x_a are the activity coefficient and the molar fractions of P_4O_{10} in the phosphoric acid respectively. P^0_{sa} was derived from the Antoine equation [4], and γ_a was derived by regressing P_4O_{10} vapor concentration data shown in [5] to the equation shown in [6] as follows:

$$\log_{10} P^0_{sa} = A - \frac{B}{C + t_l} \tag{A.1.2}$$

$$\gamma_a = \exp\left\{\frac{a_a(1-x_a)^2 + b_a(1-x_a)^3}{RT_l}\right\} \tag{A.1.3}$$

Here, t_l is the liquid temperature °C, R is the universal gas constant 8.314 J mol^{-1} K^{-1}, T_l is the liquid absolute temperature (K), and each coefficient was as follows:

$$A = 9.7070, \quad B = 3822, \quad C = 201.0$$

$$a_a = -6.732\text{E}4, \quad b_a = -4.607\text{E}4$$

Here, a_a and b_a were regressed by the almost same coefficient in the temperature range of T_l = 436–491 K.

Similarly, the saturated vapor pressure P_{sw} for H_2O in arbitrary concentration of phosphoric acid in the liquid phase is derived as follows:

$$P_{sw} = P^0_{sw} \cdot \gamma_w \cdot (1 - x_a) \tag{A.1.4}$$

Here, P^0_{sw} is the pure H_2O saturated vapor pressure mmHg, γ_w is the activity coefficient of H_2O, and x_a is the molar fractions of P_4O_{10} in phosphoric acid. P^0_{sw} was derived from the Wagner equation [7], and γ_w was derived by regressing the saturated vapor pressure data of H_2O in phosphoric acid shown in [5] to the equation shown in [6] as follows:

$$\ln\left(\frac{P^0_{sw}}{P_c}\right) = (a\vartheta + b\vartheta^{1.5} + c\vartheta^3 + d\vartheta^6) \cdot \frac{1}{1-\vartheta}, \quad \vartheta = 1 - \frac{T_l}{T_c} \tag{A.1.5}$$

$$\gamma_w = \exp\left\{\frac{a_w x_a^2 + b_w x_a^3}{RT_l}\right\} \tag{A.1.6}$$

Here, the critical pressure P_c was 1.6591E5 mmHg, and the critical temperature T_c was 647.3 K and each coefficient was as follows:

$$a = -7.76451, \quad b = 1.45838, \quad c = -2.77580, \quad d = -1.23303$$

Coefficients a_w and b_w vary with temperature, and were regressed as follows about each temperature:

T_l = 373 K : $a_w = -5.499\text{E}5$, $b_w = -1.278\text{E}6$

T_l = 398 K : $a_w = -4.904\text{E}5$, $b_w = -1.695\text{E}6$

T_l = 423 K : $a_w = -5.538\text{E}5$, $b_w = -1.051\text{E}6$

T_l = 448 K : $a_w = -5.229\text{E}4$, $b_w = -5.117\text{E}6$

$T_l = 473\,\mathrm{K}: \quad a_w = -5.454\mathrm{E}4, \quad b_w = -5.263\mathrm{E}6$

$T_l = 498\,\mathrm{K}: \quad a_w = -1.230\mathrm{E}6, \quad b_w = 2.660\mathrm{E}6$

$T_l = 523\,\mathrm{K}: \quad a_w = -7.305\mathrm{E}5, \quad b_w = -3.496\mathrm{E}5$

A.2. Evaporation and condensation rates

The evaporation and condensation rates of phosphoric acid were expressed as following activation process, based on the theory of the nucleation (droplet condensation) of a two components system mentioned in Refs. [8–10]:

$$J = \tilde{c}\,\exp\left(\frac{-\Delta\tilde{G}^*}{RT}\right) \tag{A.2.1}$$

Here, J is the amount of phosphoric acid that evaporate or condensate per the unit area on an electrode surface and unit time mol s^{-1} cm^{-2}, R is the universal gas constant 8.314 J mol^{-1} K^{-1}, and J was treated as minus and plus for evaporation and condensation respectively, T is the liquid absolute temperature (K), $\Delta\tilde{G}^*$ is the activation energy (J mol^{-1}), $\tilde{c}$ is the frequency factor.

A.2.1. Evaporation rate

The free energy change $\Delta\tilde{G}_E a$ accompanied with the phase change in evaporation was derived as follows:

$$\Delta\tilde{G}_E(x_a, x_w) = x_a\Delta\mu_a + x_w\Delta\mu_w = x_a(\mu_{al} - \mu_{ag}) + x_w(\mu_{wl} - \mu_{wg})$$
$$= x_aRT\,\ln\frac{\bar{P}_{sa}}{P_{sa}} + x_wRT\,\ln\frac{\bar{P}_{sw}}{P_{sw}} \tag{A.2.2}$$

Here, x_a and x_w are the molar fraction of P_4O_{10} and H_2O in evaporating liquid phase, $\Delta\mu_a$ and $\Delta\mu_w$ are chemical potential change (J mol^{-1}) accompanied with the phase change of P_4O_{10} and H_2O. $\bar{P}_{sa}$ and $\bar{P}_{sw}$ are the saturated vapor pressure of P_4O_{10} and H_2O in the liquid phase at electrode respectively, P_{sa} and P_{sw} are saturated vapor pressure of P_4O_{10} and H_2O for the liquid phase correspond to evaporating vapor. T is liquid absolute temperature at electrode (K).

The following relation is satisfied in the liquid phase compositions for evaporating vapor:

$$x_w = 1 - x_a \tag{A.2.3}$$

The following relation was derived from Eqs. (A.2.2) and (A.2.3)

$$\Delta\tilde{G}_E(x_a) = x_aRT\,\ln\frac{\bar{P}_{sa}}{P_{sa}} + (1-x_a)RT\,\ln\frac{\bar{P}_{sw}}{P_{sw}} \tag{A.2.4}$$

$\bar{P}_{sa}$, $\bar{P}_{sw}$ and P_{sa}, P_{sw} were derived from Eqs. (A.1.1) and (A.1.4)

$$\bar{P}_{sa}(\bar{x}_a, T) = P^0_{sa}(T)\cdot\bar{x}_a\cdot\gamma_a(\bar{x}_a, T) \tag{A.2.5}$$

$$\bar{P}_{sw}(\bar{x}_w, T) = P^0_{sw}(T)\cdot\bar{x}_w\cdot\gamma_w(\bar{x}_w, T) \tag{A.2.6}$$

$$P_{sa}(x_a, T) = P^0_{sa}(T)\cdot x_a\cdot\gamma_a(x_a, T) \tag{A.2.7}$$

$$P_{sw}(x_w, T) = P^0_{sw}(T)\cdot x_w\cdot\gamma_w(x_w, T) \tag{A.2.8}$$

Here, $\bar{x}_a$ and $\bar{x}_w$ are molar fraction of P_4O_{10} and H_2O of liquid at electrode.

Eq. (A.2.4) is transformed as follows using the equations from (A.2.5) to (A.2.8), (A.1.3) and (A.1.6):

$$\Delta\tilde{G}_E(x_a) = x_aRT\,\ln\frac{\bar{x}_a\gamma_a(\bar{x}_a, T)}{x_a\gamma_a(x_a, T)} + (1-x_a)RT\,\ln\frac{\bar{x}_w\gamma_w(\bar{x}_w, T)}{(1-x_a)\gamma_w(1-x_a, T)}$$
$$= x_aRT\,\ln\frac{\bar{x}_a\gamma_a(\bar{x}_a, T)}{x_a\,\exp((a_a(1-x_a)^2 + b_a(1-x_a)^3)/RT)}$$
$$+(1-x_a)RT\,\ln\frac{\bar{x}_w\gamma_w(\bar{x}_w, T)}{(1-x_a)\exp((a_wx_a^2 + b_wx_a^3)/RT)} \tag{A.2.9}$$

In Refs. [8–10], the phosphoric acid composition of condensation was derived as a result of searching a saddle point for the free energy change that is equivalent to Eq. (A.2.2). The evaporation composition was derived at the critical point of Eq. (A.2.9) based on above.

In order to search a critical point, Eq. (A.2.9) was differentiated by x_a and substituting the result as 0, the following equation was derived:

$$4(b_a + b_w)x_a^3 + 3(-a_a - 3b_a + a_w - b_w)x_a^2 + 2(2a_a$$
$$+3b_a - a_w)x_a - a_a - b_a + RT\,\ln\frac{(1-x_a)\bar{x}_a\gamma_a}{x_a\bar{x}_w\gamma_w} = 0 \tag{A.2.10}$$

P_4O_{10} molar fraction in the evaporated phosphoric acid was derived by solving the above equation with x_a numerically. The activation energy $\Delta\tilde{G}^*_E$ was derived as the free energy change on critical point by substituting x^*_a for x_a in Eq. (A.2.9) as follows:

$$\Delta\tilde{G}^*_E = \Delta\tilde{G}_E(x^*_a) = x^*_aRT\,\ln\frac{\bar{x}_a\gamma_a(\bar{x}_a, T)}{x^*_a\exp((a_a(1-x^*_a)^2 + b_a(1-x^*_a)^3)/RT)}$$
$$+(1-x^*_a)RT\,\ln\frac{\bar{x}_w\gamma_w(\bar{x}_w, T)}{(1-x^*_a)\exp\left(\left(a_wx^*_a + b_wx^{*3}_a\right)/RT\right)} \tag{A.2.11}$$

Here, the free energy change direction was determined so as to satisfy that the evaporation direction becomes minus for J in Eq. (A.2.1), and as a result of this, the following relation was satisfied:

$$-\Delta\tilde{G}^* = \Delta\tilde{G}^*_E \tag{A.2.12}$$

The frequency factor $\tilde{c}_E$ was derived as follows:

$$\tilde{c}_E = c_E\cdot\beta_{aE}\cdot S\cdot c_{wl} \tag{A.2.13}$$

Here, c_E is frequency factor coefficient, S is area ratio that derived by dividing surface area of electrode by appearance surface and treated as 1. c_{wl} is H_2O molar concentration in liquid phase at the electrode mol cm^{-3}. β_{aE} is collision rate of P_4O_{10} in liquid phase at the electrode and derived assuming Herz–Knudsen equation for condensation [11] as follows:

$$\beta_{aE} = \frac{x_a}{\sqrt{2\pi M_akT}} \tag{A.2.14}$$

Here, x_a is the molar fraction of P_4O_{10} in the liquid phase, M_a is the molecular weight of P_4O_{10}, k is the Boltzmann constant 1.38E−23 J K^{-1}, and T is the liquid phase absolute temperature (K).

Consequently, the evaporation rate is derived adopting activation energy (A.2.12) and frequency factor (A.2.13) as follows:

$$J_E = \tilde{c}_E\,\exp\left(\frac{\Delta\tilde{G}^*_E}{RT}\right) \tag{A.2.15}$$

A.2.2. Condensation rate

According to the same manner for the evaporation rate, the activation energy $\Delta\tilde{G}^*_C$, frequency factor $\tilde{c}_C$, collision rate in the vapor phase β_{aC}, and condensation rate J_C were derived as follows:

$$\Delta\tilde{G}^*_C = \Delta\tilde{G}_C(x^*_a) = -x^*_aRT\,\ln\frac{P_a}{P^0_{sa}x^*_a\exp((a_a(1-x^*_a)^2 + b_a(1-x^*_a)^3)/RT)}$$
$$-(1-x^*_a)RT\ln\frac{P_w}{P^0_{sw}(1-x^*_a)\exp\left(\left(a_wx^{*2}_a + b_wx^{*3}_a\right)/RT\right)} \tag{A.2.16}$$

$$\tilde{c}_C = c_C\cdot\beta_{aC}\cdot S\cdot c_{wg} \tag{A.2.17}$$

$$\beta_{aC} = \frac{P_a}{\sqrt{2\pi M_akT}} \tag{A.2.18}$$

$$J_C = \tilde{c}_C \exp\left(\frac{\Delta\tilde{G}_C^*}{RT}\right) \quad (A.2.19)$$

Here, P_a and P_w are the partial pressure of P_4O_{10} and H_2O in condensing vapor phase phosphoric acid; c_C is the frequency factor coefficient, c_{wg} is the molar concentration of H_2O in vapor phase mol cm^{-3}, β_{aC} is the collision rate of P_4O_{10} in the vapor phase at process gas.

Appendix B. B. Unsteady phosphoric acid balance

The balance of phosphoric acid between the liquid phase in electrode and the vapor phase in process gases were regarded as the P_4O_{10} balance and H_2O balance separately.

The balance for P_4O_{10} was derived as follows:

$$V\frac{dc_{al}}{dt} = A \cdot J \cdot x_a^* \quad (B.1)$$

$$q_{in} \cdot c_{ag_{in}} = A \cdot J \cdot x_a^* + q_{out} \cdot c_{ag_{out}} \quad (B.2)$$

Here, V and A are the volume (cm^3) and surface area (cm^2) of the electrode element respectively. J is the evaporation or condensation rate of phosphoric acid (mol cm^{-2} s^{-1}), x_a^* is the molar fraction of P_4O_{10} in the evaporating or condensing phosphoric acid vapor, c_{al} is the molar concentration of P_4O_{10} in liquid phase phosphoric acid at electrode. The q_{in} and q_{out} are the volume flow rate of the process gases at the inlet and outlet of the electrode element channel respectively (cm^3 s^{-1}), $c_{ag_{in}}$ and $c_{ag_{out}}$ are the molar concentration of P_4O_{10} in vapor phase phosphoric acid at the inlet and outlet on the element channel respectively (mol cm^{-3}).

The balance for H_2O is derived as following:

$$V\frac{dc_{wl}}{dt} = A \cdot J \cdot (1 - x_a^*) \quad (B.3)$$

$$q_{in} \cdot c_{wg_{in}} = A \cdot J \cdot (1 - x_a^*) + q_{out} \cdot c_{wg_{out}} \quad (B.4)$$

Here, c_{wl} is H_2O molar concentration (mol cm^{-3}) in liquid phase phosphoric acid at electrode; $c_{wg_{in}}$ and $c_{wg_{out}}$ are the molar concentration of H_2O in the vapor phase phosphoric acid at the inlet and outlet of the element channel respectively (mol cm^{-3}).

The difference equations for the equations from (B.1)–(B.4) were calculated at the unsteady loop that including the electrochemical reaction, heat transfer, and gas flow also, and consequently the molar amount of P_4O_{10} and H_2O in the electrode element in each time step were calculated as $V \times c_{al}$ and $V \times c_{wl}$ respectively. The mol concentration of P_4O_{10} and H_2O in the vapor phase process gases in each time step were calculated as $(c_{ag_{in}} + c_{ag_{out}})/2$ and $(c_{wg_{in}} + c_{wg_{out}})/2$ respectively.

References[1]

[1] S. Yoshioka, K. Mitsuda, H. Horiuchi, M. Matsumoto, DENKI KAGAKU 65 (4) (1997) 314–319.
[2] S. Yoshioka, K. Mitsuda, H. Horiuchi, M. Matsumoto, DENKI KAGAKU 66 (1) (1998) 41–47.
[3] H. Hirata, M. Hori, Journal of Power Sources 63 (1996) 115–120.
[4] J.H. Dean, Lange's Handbook of Chemistry (1973) 10–28.
[5] E.H. Brown, C.D. Whitt, Industrial and Engineering Chemistry 44 (3) (1952) 615–618.
[6] J.M. Prausnitz, Molecular Thermodynamics of Fluid Phase Equilibria (1985) p. 192.
[7] Chemical Society of Japan, The Chemistry Manual Basic, vol. II, (1993) p. II-117.
[8] H. Reiss, Journal of Chemical Physics 18 (6) (1950) 840–848.
[9] W. Studzinski, et al., Journal of Chemical Physics 84 (7) (1986) 4008–4014.
[10] M. Kulmala, et al., Journal of Chemical Physics 93 (1) (1990) 696–701.
[11] T. Keii, Reaction Kinetics (1983) p. 88.

[1] Product names mentioned herein may be trademarks of their respective companies.